Nanomed J. 11(3):250-267, Summer 2024

RESEARCH PAPER

Equisetum ramosissimum desf-assisted green synthesis of cerium oxide nanoparticles: Characterization and antimicrobial potential against cariogenic *Streptococcus mutans*

Mansour Hadi Mohammed [1]*, Bayan Abdullah Hasan [1]

[1]*Pedodontic,Orthodontic, Preventive department, college of dentistry, Hawler Medical University, Erbil 44001, Iraq*

ABSTRACT

Objective(s): This study explores the biosynthesis of cerium oxide nanoparticles using aqueous extract of *Equisetum ramosissimum Desf* as both a reducing and stabilizing agent and evaluates its antibacterial activity against cariogenic *streptococcus mutans*.

Materials and Methods: Cerium oxide nanoparticles were synthesized and characterized using UV-VIS, FTIR, XRD, FESEM, EDX, DLS, and Zeta potential analyses. Antibacterial activity against *S. mutans* was evaluated via the agar well diffusion method.

Results: Optical analysis revealed an absorption peak within the 307–314 nm range, suggesting a bandgap value of 3.04–3.37 eV. FTIR analysis confirmed Ce-O stretching vibrations and bonds with phytochemicals from the *E.ramosissimum Desf* extract on the nanoparticle surfaces. XRD showed a cubic fluorite structure with a crystalline size of 5.99–11.74 nm. FESEM imaging depicted uniform, nearly spherical nanoparticles with estimated sizes ranging from 22 to 31 nm. The EDX spectrum indicated the presence of cerium and oxygen signals, affirming the purity of the fabricated nanoparticles. DLS results corroborated the average nanoparticle size (28.11–54.61 nm), in agreement with FESEM findings and zeta potential values (-11.4 to 29.2 mV) indicating moderate stability of nanoparticles. Antibacterial assays showed significant inhibition zones (20–32 mm) against *S. mutans*.

Conclusion: The green-synthesized CeO_2-NPs exhibit promising antimicrobial efficacy against *S. mutans*, suggesting their potential for dental applications. Furthermore, employing plant extract for cerium salt reduction presents a promising avenue for reducing the environmental impact associated with chemical synthesis.

Keywords: *Ceric oxide, Dental caries, Nanoparticles, Phytochemicals Streptococcus mutans*

How to cite this article

Mohammed MH, Hasan BA. Equisetum ramosissimum desf-assisted green synthesis of cerium oxide nanoparticles: Characterization and antimicrobial potential against cariogenic Streptococcus mutans. Nanomed J. 2024; 11(3): 250-267. DOI: 10.22038/NMJ.2024.77376.1886

INTRODUCTION

Dental caries is a multifactorial oral disease that causes demineralization of dental hard tissues. According to data provided by the World Health Organization (WHO), the prevalence of dental caries ranges from 60 to 80% in children and about 100% in adults [1]. *Streptococcus mutans* is well recognized as the primary oral bacteria responsible for the formation of dental caries [2]. It primarily functions by producing sticky and insoluble extracellular polysaccharides, such as glucan, using the glycosyltransferase (GTF) enzyme which results in the creation of a biofilm on the tooth surface [3]. Despite many successful protocols that have been implemented to prevent and control dental caries, it remains a popular oral health problem in some countries [4, 5]. Furthermore, antimicrobial agents that have been reported so far to decrease the occurrence of dental caries may have side effects [6]. Considering the development of bacterial resistance to antibacterial agents [7], it is crucial to search for new antimicrobial agents that have minimal side effects and do not induce bacterial resistance mechanisms. In light of this, nanotechnology is regarded as a formidable asset.

With the advancement of nanotechnology, researchers have made substantial progress in

* *Corresponding author: Email: Mansour.mohammed@hmu.edu.krd*

Note. This manuscript was submitted on January 8, 2024; approved on March 4, 2024

creating new antimicrobial materials for biomedical applications. Among these, metal and metal oxide nanoparticles stand out. Their ability to combat microbes stems from their small size and large surface area compared to their volume. These properties allow them to strongly interact with bacterial membranes, resulting in a wide range of antimicrobial effects beyond just releasing metal ions[8,9]. Many different nanoparticles have been tested against microbes for their antimicrobial efficacy including AgO, Ag_2O, Al_2O_3, TiO_2, ZnO, CuO, Co_3O_4, In_2O_3, MgO, SiO_2, ZrO_2, Cr_2O_3, Ni_2O_3, Mn_2O_3, CoO, NiO, and CeO_2 [10].

Several in-vitro studies have investigated the antimicrobial efficacy of plant-mediated nanoparticles against oral pathogens. Zinc oxide derived from *Avicennia marina mangrove* leaves exhibited significant antibacterial activity against *Streptococcus mutans* [11]**.** Similarly, titanium dioxide nanoparticles, in combination with grape seed extract, demonstrated enhanced antibacterial effects against *Streptococcus mutans* and *Lactobacillus* [12]**.** Additionally, biologically synthesized silver nanoparticles showed notable antibacterial effects against *Escherichia fergusonii* and *Streptococcus mutans* [13]. In another study, the stannous nanoparticles mediated by *Citrullus lanatus* demonstrated effectiveness against *Streptococcus mutans* [14]**.**

Cerium, an abundant rare earth metal classified within the lanthanide series of the periodic table, exhibits dual valence states—trivalent (Ce3+) and tetravalent (Ce4+)—giving rise to cerium dioxide (CeO_2) and cerium sesquioxide (Ce_2O_3). Cerium oxide nanoparticles exhibit outstanding capabilities in antioxidation, redox reactions, and antibacterial effects, as well as versatile applications spanning magnetic, optical, electrochemical, physicochemical, and biomedical fields [15, 16].

Several investigations have detailed both chemical and physical methodologies to produce metal and metal oxide nanoparticles. However, these techniques rely on harmful reducing solvents, posing significant risks to biodiversity and ecosystems. Additionally, nanoparticles produced through these methods tend to be toxic and unstable, reducing their efficacy. Consequently, researchers have recently turned to a safer, less toxic approach referred to as Green Synthesis. This approach utilizes diverse biological resources like plants, microbes, or their derivatives, which contain abundant phytochemicals like phenolic compounds, amines, enzymes, and flavonoids. These compounds are thought to contribute to the reduction of bulk salts, facilitating the stabilization of resulting nanoparticles [17-19].

The medicinal plant *Equisetum ramosissimum Desf,* commonly known as 'Horsetail' and a member of the Equisetaceae family, is distributed globally. Traditionally, its aerial parts considered an herbal remedy, have been used for treating various conditions, including urinary-related issues like kidney stone formation, stomachaches, skin disorders, bone fractures, joint pains, and rheumatism. Rather than its application in urinary tract infections (UTIs), this plant has been utilized for addressing inflammation, respiratory ailments, gastrointestinal troubles, skin conditions (itching, scabies), gonorrhea, rheumatism, female fertility, back pain, muscle ache, fever, sunstroke, and blood pressure regulation[20-22]. Studies have highlighted *Equisetum ramosissimum's* richness in phytochemicals, encompassing saponins, flavonoids, alkaloids, phenolic compounds, and tannins [23-25].

This study focused on synthesizing CeO_2 nanoparticles via green synthesis, employing different concentrations of *E. ramosissimum Desf* extract. Additionally, the research evaluated the antibacterial effectiveness of these nanoparticles against clinically isolated cariogenic *Streptococcus mutans.* To our knowledge, this is the first study detailing the green synthesis of CeO_2 nanoparticles utilizing *E. ramosissimum Desf* extract.

MATERIALS AND METHODS

Materials and reagents

Cerium nitrate hexahydrate (Ce (NO3)3·6H2O), sodium hydroxide (NaOH), brain heart infusion broth (BHI), and Mueller Hinton Agar (MH) were obtained from Sigma Aldrich. Throughout the experimental processes, deionized and double distilled water were used.

Methods

Preparation of Equisetum ramosissimum Desf aqueous extract

The aerial parts of *E.ramosissimumDesf* were gathered from Choman Town, situated in Erbil city within the Kurdistan region of Iraq. To ensure their precise identification, the plant specimens underwent thorough examination and validation at the Herbarium of the Department of Biology,

College of Sciences, Salahaddin University - Erbil. Following collection, the aerial materials were meticulously cleaned and subsequently shade-dried under room temperature conditions for seven days. Subsequently, these dried materials were finely powdered. The preparation of the *E. ramosissimum Desf* aqueous extract is done by mixing 30 g of powdered plant material with 150 mL of distilled water in a 5:1 ratio. This mixture was then agitated for 8 hr at a temperature of 40°C with a speed of 150 rpm. The resulting solution underwent a double filtration process using Whatman paper No. 1[25]. The filtrate obtained from this process was kept in a sealed container at 4°C for subsequent use.

Phytochemical analysis of the plant extract

The preliminary phytochemical screening of E. ramosissimum Desf extract was done to confirm the presence of different phytochemicals like flavonoids(sodium hydroxide test), alkaloids(Hager's test), phenols and tannins(ferric chloride test), and saponins (frothing test) using standard procedures [26]. Furthermore, the plant extract was characterized by UV-VIS spectroscopy using a Shimadzu double-beam spectrophotometer (model UV-1800, Kyoto, Japan) and ATR-FTIR spectroscopy using ALPHA II BRUKER (model COMPACT -PLATINUM-ATR).

Green synthesis of cerium oxide nanoparticles

The synthesis of cerium oxide nanoparticles through plant mediation using *E.ramosissimumDesf* extract followed a previously reported method [29], with slight adjustments. To prepare a 1M solution of cerium nitrate hexahydrate, a total of 4.38 g of salt was dissolved in 10 mL of deionized water using a magnetic stirrer hot plate. Four different volumes of plant extract were used in this experiment. To prepare group 1 (0.5:1 v/v ratio), 5 mL of plant extract was added dropwise to 10 mL of precursor solution under continuous stirring (1500 RPM) at 65 °C for 2 hr. At that time, pH of the solution was adjusted to 7-8 using 1M sodium hydroxide (NaOH) solution. During this period, the color change of solution was monitored. After 2 h, the obtained gel underwent multiple washes using deionized water and ethanol and was dried in an oven at 90 ˚C to thicken the gel. The obtained gel was then calcined using a RENFERT Magma furnace at 400 ˚C for 2 hr [27-30] Finally, the obtained product was ground by mortar and pestle to form a fine powder and subjected to further characterization. Accordingly, there were 4 groups in this experiment:

Group A: 0.5:1 V/V (5 mL of plant extract added to 10 mL of cerium nitrate salt)
Group B: 1:1 V/V (10 mL of plant extract added to 10 mL of cerium nitrate salt)
Group C: 1.5:1 V/V (15 mL of plant extract added to 10 mL of cerium nitrate salt)
Group D: 2:1 V/V (20 mL of plant extract added to 10 mL of cerium nitrate salt)

Characterizations

UV-Visible spectroscopy

The UV-visible spectroscopy technique was used to characterize the optical characteristics and band gap energy of the green cerium oxide nanoparticles within the wavelength range of 250–800 nm. The analysis was performed utilizing a Shimadzu double-beam spectrophotometer (model UV-1800, Kyoto, Japan) with a 1 nm resolution. The band gap energy was determined using the Tauc relation, which was calculated based on the absorption spectra of the nanoparticles as follows:

$$\alpha h\nu = A (h\nu - Eg)n$$

Where α is the optical absorption coefficient, *hv* is the photon energy, *Eg* is the band gap and *A* is an energy-independent constant and n is 2 or 0.5 for direct or indirect transitions, respectively. It has been proven that the cerium oxide nanoparticles had a direct transition, therefore the value of 2 is selected here [31].

Fourier transform infrared spectroscopy (FTIR)

to examine functional groups within the plant extract, serving as a capping agent, and to verify the production of green nanoparticles, FTIR spectroscopic analysis was conducted. This analysis employed the Attenuated Total Reflectance FTIR (ATR-FTIR) methodology utilizing the COMPACT ALPHA II BRUKER-PLATINUM-ATR model.

X-ray diffraction (XRD)

The crystal structure as well as the purity of the CeO_2-NP was recorded using an X-ray diffractometer (Ultimate IV XRD system, Rigaku Corporation, Tokyo, Japan) at room temperature and interpreted using Xpert Highscore plus (software version 5.2.0) and its associated powder database PDF-2 Database Copyright International Center for Diffraction Data (ICDD-2013) and

crystallography open database (COD-2023). The crystallite size of CeO_2 NPs was determined using Scherrer's equation ($D=0.9\lambda/\beta\cos\theta$) and analyzed with Origin software. In this equation, D represents the average size of the crystalline domain perpendicular to the reflecting planes, λ is the X-ray wavelength (1.5406 Å), β is the angular full width at half maximum in radians, and θ is the diffraction angle (2θ is the measured angle of diffraction in degrees) or Bragg's angle. [32].

Field emission scanning electron microscopy (FESEM) & Energy-dispersive X-ray spectroscopy (EDX)

The size and morphology of the prepared particles were analyzed using scanning electron microscopy, Hitachi S4160FE-SEM operating at 20 Kv. To measure the size of nanoparticles, the size of 200 particles was measured from FE-SEM image using Image J software (version 1.8.0) and the average particle size for each sample was estimated by fitting the particle size distribution histogram to the log-normal distribution function, as described by Paswan, Kumari [33].

Furthermore, to analyze the qualitative chemical and elemental composition of prepared particles, energy-dispersive X-ray spectroscopy was carried out coupled to FE-SEM operated at 20 Kv, and data was recorded and analyzed using TEAM™ EDS Analysis System.

Dynamic light scattering analysis

The zeta potential charge (ZPC) and approximate hydrodynamic diameter of the CeO_2-NPs were determined using Litesizer 500 (Anton Paar-serial number: 82807900).

Antibacterial activity of CeO_2 NPs

The antibacterial properties of *E. ramosissimum Desf.* mediated- CeO_2 nanoparticles were investigated against clinically isolated *Streptococcus mutans* using the agar well diffusion method with minor adjustments [34].

Agar well diffusion assay

Clinically isolated *Streptococcus mutans* (PP061004 blasted at NCBI) after its isolation and identification regrowth in sterile brain heart infusion broth (BHI). Using a sterile loop, a single colony of bacteria was introduced into 5 mL of sterile BHI broth and incubated at 37 °C for 24 hr. Following the incubation of bacteria, the optical density (OD) of broth was adjusted to 0.5 McFarland using an EMCLAB spectrophotometer at 600nm.

Following adjustment of bacterial density to 1×10^8 CFU/Ml (OD=0.11), 100 µL of 24h mature broth culture of bacteria spread over the surface of already prepared Mueller-Hinton Agar plate using cotton swabs in different directions. Using a sterile cork borer, a 6 mm well was made at the surface of each Petri- plate at a 2 cm distance. The antibacterial activity was evaluated using six different concentrations of CeO_2 nanoparticles: 2000, 1000, 500, 250, 125, and 62.5 µg/mL. The samples were prepared by dispersion of cerium oxide nanoparticle powder in deionized water and sonicated for 20 minutes. Using a sterile micropipette, 0.05 mL of a solution containing different concentrations of nanoparticles was added to each well. Chlorhexidine was used as a positive control. Subsequently, the plates that had been inoculated were placed in an incubator set at a temperature of 37 °C for a duration of 24 hr. After incubation time, the clear zone's diameter around each well was measured and quantified in millimeters to represent its antibacterial efficacy. The experiment was assessed in quintuplicate and the average results were determined for the antibacterial activity. The mean, standard deviation, and P value of the inhibition zone were analyzed using Graph Pad Prism (version 9).

RESULTS AND DISCUSSION

Phytochemical analysis of the plant extract

The qualitative analysis of secondary metabolites in *E. ramosissimum Desf* revealed the presence of the assessed compounds, as outlined in the Table 1. Previous research has similarly documented the existence of various phytochemicals in different components of *E. ramosissimum,* corroborating the findings presented in this study[23-25, 35]. Furthermore, UV–Vis absorption spectra of plant extract exhibit two prominent absorption bands at 242 nm and 418 nm, while also demonstrating a less intense absorption at 296 nm as depicted in Fig. 1. Typically, UV/VIS absorption bands of flavonoids and phenolic acids manifest as two distinct absorption bands, one falling between 230-280 nm and the other between 300-380 nm[36-38]. Hence, the detection of absorption peaks within the wavelength range of 230-420 nm in the aqueous extract spectra serves as evidence for

Table 1. Qualitative phytochemical screening of E. ramosissimum Desf extract

Phytochemicals	Experiment	Observations	Result
Flavonoids	Sodium hydroxide test	The deep yellow-orange color became colorless after the addition of HCL	+ve
Phenols	Ferric chloride test	Black-blue coloration	+ve
Tannins	Ferric chloride test	Black-blue coloration	+ve
Saponins	Foam test	Foam at the top of the liquid remains for a while	+ve
Alkaloids	Hager's test	Yellow colored precipitate	-ve

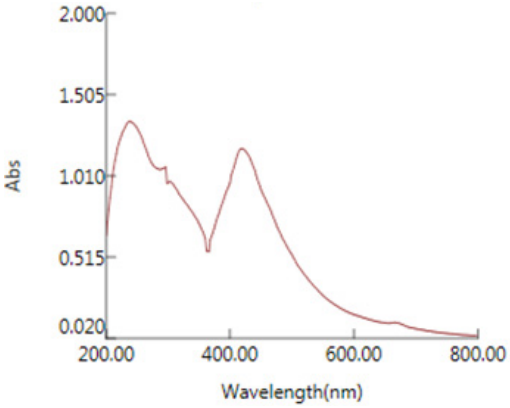

Fig. 1. UV/VIS spectrum of E. ramosissimum Desf extract

the existence of a blend of active phenolic acids, flavonoids, and associated chemicals present in the samples.

Preparation of cerium oxide nanoparticles

This method verified the successful green synthesis of cerium oxide nanoparticles by noting a color change in the cerium salt solution. The solution visibly shifted from a yellow-orange hue to a dark-brown color upon the introduction of the plant extract in all groups, Fig. 2.

This observation is indicative of the reduction of Ce4+ to Ce0. Following the washing and subsequent drying of the gel, it underwent additional calcination at a temperature of 400 ˚C, resulting in the production of cerium oxide powder with yellow coloration. Cerium has been shown to occur in two oxidation states, namely Ce (III) and Ce (IV). It is commonly observed that Ce (III) exhibits a colorless appearance, whereas Ce (IV) displays a yellow to red coloration [39-41]. Therefore, nanoparticles produced in our method were made of Ce (IV) as seen by their yellow color, Fig. 3.

Fig. 3. Yellow-colored cerium oxide nanoparticle powder

Characterizations

UV-visible analysis

It is well-documented that cerium, in its dual oxidation states, demonstrates the absorption of ultraviolet (UV) light, evident through two separate absorption peaks. Specifically, one absorption peak occurs within the wavelength

Fig. 2. Color change following reduction of nanoparticles, A : before and B : after reduction

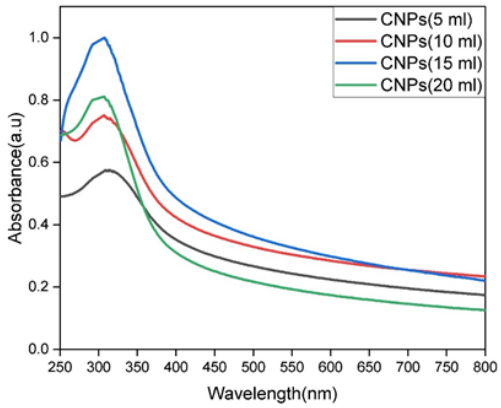

Fig. 4. UV/VIS spectrum of CeO_2 nanoparticles

range of 230 to 260 nanometers, corresponding to the Ce(III) state, while the second absorption peak falls within the wavelength range of 300 to 400 nanometers, corresponding to the Ce(IV) state [41]. Therefore, nanoceria prepared by our method were made of Ce (IV).

In this study, absorption peaks for different plant extract concentration biosynthesized CeO_2-NPs were seen at wavelengths of 314 nm, 310 nm, 307 nm, and 309 nm, respectively, as depicted in Fig. 4. A previous study showed the presence of a comparable absorption peak at a wavelength around 300-330 nm for biosynthesized CeO_2-NPs [28, 42-44].

Additionally, during this evaluation, the optimal concentration of *E.ramosissimum Desf* extracts for synthesizing the highest quantity of CeO_2-NPs with dimensions less than 50 nm was identified. The CeO_2 nanoparticles synthesized using *E.ramosissimum Desf* extracts at a concentration of 1.5:1 (v/v) exhibited the highest absorption peak at 307 nm. The more the absorbance value that was produced by the nanoparticles, the greater the quantity of nanoparticles that were generated [45]. It is important to point out that a concentration of 1.5% of *E. ramosissimum Desf* extracts was determined to be the optimal concentration for the synthesis of CeO_2 NPs.

The band gap energy values for CeO_2-NPs were determined to be 3.14, 3.27, 3.37, and 3.04 eV, respectively, as illustrated in Fig. 5. The value of band gap energy increased when the concentration of *E. Ramosissimum Desf* extract was elevated from a ratio of 0.5:1 to 1.5:1 v/v which confirmed the formation of smaller nanoparticles. The reduction in particle size could be attributed to a higher percentage of phytochemicals present within the plant extract which prevent particles from aggregation. On the other hand, increasing plant extract up to 20 mL (2:1 v/v) creates nanoparticles of larger size and smaller bandgap energy which might be related to the higher viscosity of solution, a pattern that has also been noted in some earlier investigations [28, 46].

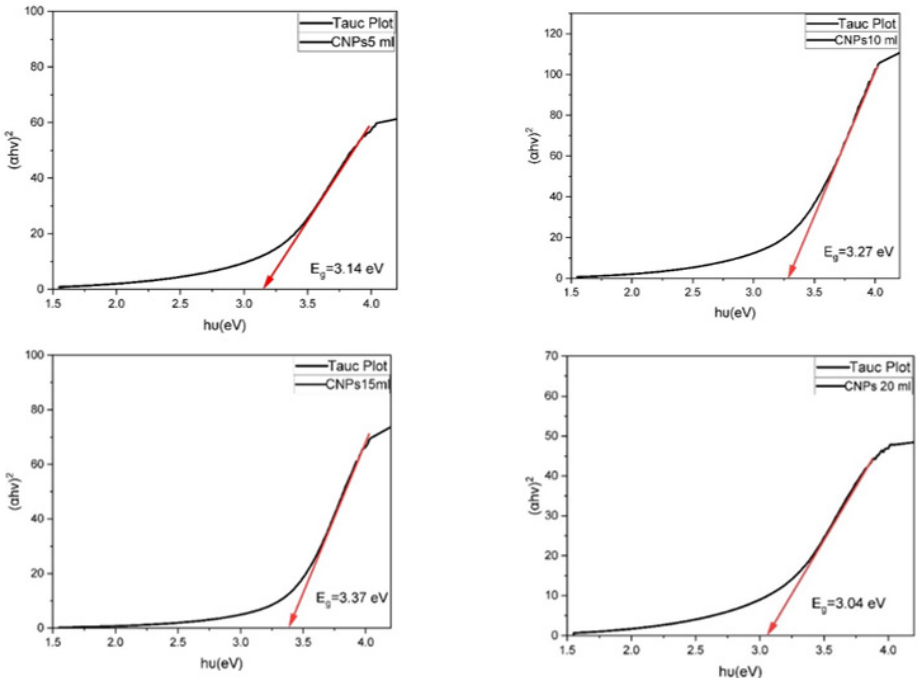

Fig. 5. Band gap energy of *E. Ramossisum Desf* mediated CeO_2 NPs

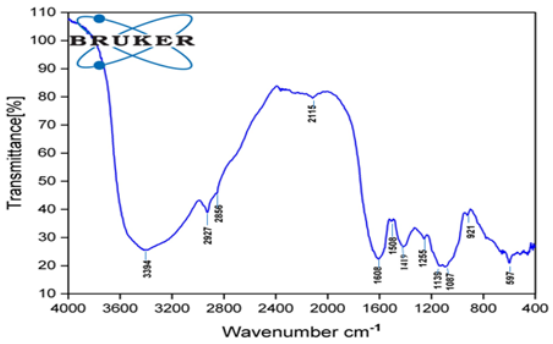

Fig. 6. FTIR spectrum of pure *E. Ramosissemum Desf* extract

FTIR analysis

In the spectrum of pure *E. Ramosissemum Desf* extract, as shown in Fig. 6, the broadband at 3394.72 cm^{-1} contributes to the stretching vibration of O–H bonds [38, 47], doublet band at 2927.94 cm^{-1} and 2856.58 cm^{-1} represent C–H stretching vibrations, characteristic to CH_3 and CH_2 groups of aliphatic compounds[48, 49],. Furthermore, bands at 1608.63 cm^{-1}, 1508.33 cm-1, 1419.61 cm^{-1}, and 1255.66 cm^{-1} were of C-O stretching vibrations in the CHO group, Amide II N-H deformation as well as the presence of C=C bonds, bending vibration of C–H bond of CH3 and CH_2 groups and C–O stretching vibration of organic compound respectively [38, 49, 50].

Finally, bands at 1139.93 cm^{-1}, 1087.85 cm^{-1}, and 921.97 cm^{-1} related to C-O, C=C, and C-O-C groups stretching of carbohydrates and bending vibration of C-H bond [48, 51]. The O–H, C-H, and N–H are the primary functional groups present in phytochemicals such as proteins, phenolic compounds, vitamins, flavonoids, alkaloids, terpenes, tannins, and saponins [29].

After the formation of cerium oxide nanoparticles, some bands of E. Ramosissemum Desf extract 3394.72, 1608.63, 1139.93, and 1087.85 shifted to lower wavelengths of 3305, 1588, 1130, and 1059 cm^{-1} respectively, as shown in Fig. 7. Broad band at 3305 cm^{-1} attributed to stretching vibration of hydroxyl groups of organic compound as flavonoids or adsorbed water that exist in the surface of nanoparticles, band at 1588 cm^{-1} is assigned to C-H stretching of CH_2 group of aliphatic compound [52, 53], band at 1130 cm^{-1} and 1059 cm^{-1} due to C=O and C–O–C groups stretching vibration respectively [53, 54]. The appearance of these peaks at the surface of nanoparticles indicates the direct involvement of -C-O, -C, -H, and OH functional groups of phytochemicals in the capping and stabilization of the CeO_2NP.

Furthermore, two more new peaks appear at 1346 cm^{-1} and 1788 cm^{-1} which might correspond

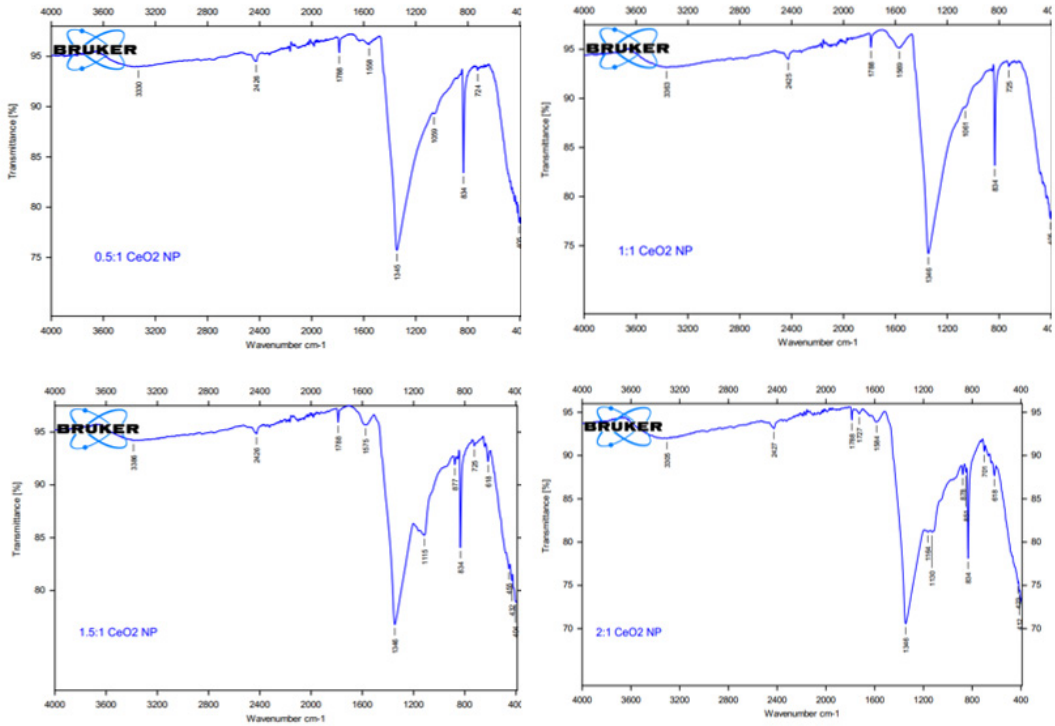

Fig. 7. FTIR spectrums of CeO_2NPs

to O-H bending and C=O stretching vibration that belongs to the residual combinations of *E. Ramosisse*mum Desf extract, respectively. The remaining peaks of plant extract, 2927.94 cm^{-1}, 2856.58 cm^{-1}, 1508.33 cm^{-1}, 1419.61 cm^{-1}, 1255.66 cm^{-1}, and 921.97 cm^{-1} were abolished in the nanoparticle spectrum, indicating that the respective groups had a direct interaction with Ce ions, causing its oxidation and thus being not appearing on the surface of nanoparticles.

Metal oxide nanoparticles generally had absorption bands below 1000 cm^{-1} because of the inter-atomic vibrations [55]. In our study, Ce–O stretching vibrations were observed at a range between 400-850 cm^{-1}, as shown in Fig. 7. In group 1 absorption bands were at 405, 724, and 834 cm^{-1}, group 2 at 405,725 and 834 cm^{-1}, group 3 at 404,432,455,618,725 and 834 cm^{-1}, and group 4 at 412,423,618,701, 834 and 851 cm^{-1} respectively. Similar to our study Ce–O stretching vibrations were observed at ~410 cm^{-1} [55], ~ 425 cm^{-1} (52), ~450 cm^{-1} [56-58], ~620 cm^{-1} [55], ~725 cm^{-1} [59, 60],~ 830 cm^{-1} [59, 61-63] and ~850 cm^{-1} [46, 60, 64]. Compared to the results of previous studies, the detection of distinct absorption bands associated with Ce-O vibrations serves as confirmation that the generated particles indeed cerium oxide.

XRD analysis

Fig. 8 displays the XRD pattern of CeO_2NPs produced using different concentrations of *E. ramosissimum Desf* extract. It reveals the Presence of several broad Bragg peaks at the 2ϑ position of 28.57, 33.10, 47.51, 56.38, 59.13, 69.46, 76.74, 79.11, 88.49, 95.46 corresponding to Miller indices, hkl (111), (200), (220), (311), (222), (400), (331), (420), (422) and (511) well matched to

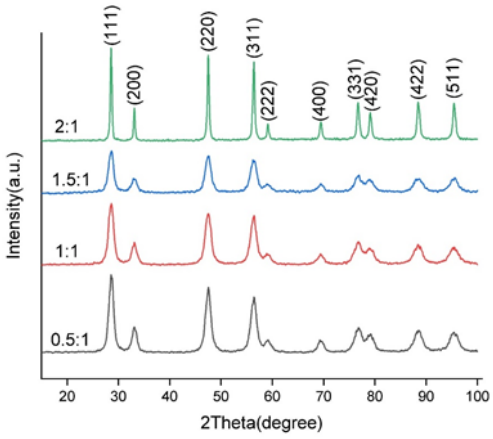

Fig. 8. XRD patterns of 4 groups of cerium oxide nanoparticles

International Centre for Diffraction Data (ICDD) card no: 34-0394, which were represented the typical face-center cubic fluorite structure of CeO_2 NPs with a space group of Fm3m (number.225), consistent with the findings from the prior experiments [44, 65, 66], confirming successful formation of cerium oxide nanoparticles.

It was observed that there are no other diffraction peaks detected in the XRD pattern indicating the purity of fabricated nanoparticles. In addition, it was found that diffraction peaks showed high intensity suggesting that green synthesized cerium oxide nanoparticles possess excellent crystalline characteristics. These findings resoundingly support the extract's role in enhancing the purity and crystallinity of the sample of as-produced cerium oxide [58, 67].

Similar to results reported by previous studies, diffraction peaks became broader (intensities reduced as appeared in (Fig. 8) as the concentration of plant extract increased indicating the decrease in crystalline size [27-29]. The decrease in the size of the crystals may be due to the presence of phytochemicals during the production phases of nanoparticles which decreases the nucleation and subsequent growth rate of the nanoparticles [52, 53].

In the present study, the Crystal size for *E. Ramosissimum Desf* mediated-CeO_2-NPs was 8.02 nm, 6.92 nm, 5.99nm, and 11.74 nm respectively. Crystal size was decreased as the concentration of plant extract increased up to (1.5:1v: v). On the other hand, increasing the percentage of extract to 2:1 increases the size of the crystal which might be caused by an increase in crystallite with fewer lattice flaws, which would result in a decrease in grain boundaries[29]. These results indicate a strong relationship between the concentration of the extract and the observed changes in crystalline size, confirming the earlier discussion by UV/VIS spectroscopy.

The crystallite size of the cerium oxide nanoparticles produced by our method was found to be very small compared to green CeO_2-NPs reported previously [46, 68-70]. The reduced crystallite size of biosynthesized CeO_2-NPs is most effective in enhancing photocatalytic and antibacterial activities(71). The current study demonstrates that the (1.5:1 v/v) *E. Ramosissimum Desf* CeO_2-NPs, with a small crystallite size of 5.99 nm have the potential to significantly enhance both the photocatalytic and antibacterial properties.

FESEM and EDX analysis

Fig. 9 displays FESEM images of all samples at

60,000X magnification. As shown in the figure, the produced nanoparticles of all groups reveal that the particles are of nanoscale size and exhibit uniformity, with an almost spherical. It was clear from the images that particles tended to agglomerate. Putri and Rilda [58] reported the bioproduction of CeO_2 nanoparticles using Moringa oleifera leaf extract in which agglomeration of particles occurs as well. A similar pattern occurs in the biosynthesize of CeO_2 nanoparticles using *Morinda citrifolia L. fruit extracts* [45].

The average particle size for samples was estimated to be 25.38 nm, 24nm, 22 nm, and 31 nm along with a standard deviation of 1.22nm, 1.27 nm, 1.30 nm, and 1.29 nm respectively, as appeared in the Fig. 9. The average size of the particle was found to be decreased with an increase in plant extract concentration from 5-15 mL confirming the earlier results by UV/VIS spectroscopy and XRD patterns. In accordance with our study, Elahi and Mirzaee [28] conducted the green synthesis of cerium oxide nanoparticles utilizing different concentrations of *Salvia Macrosiphon Boiss* seeds Extract. Their FESEM

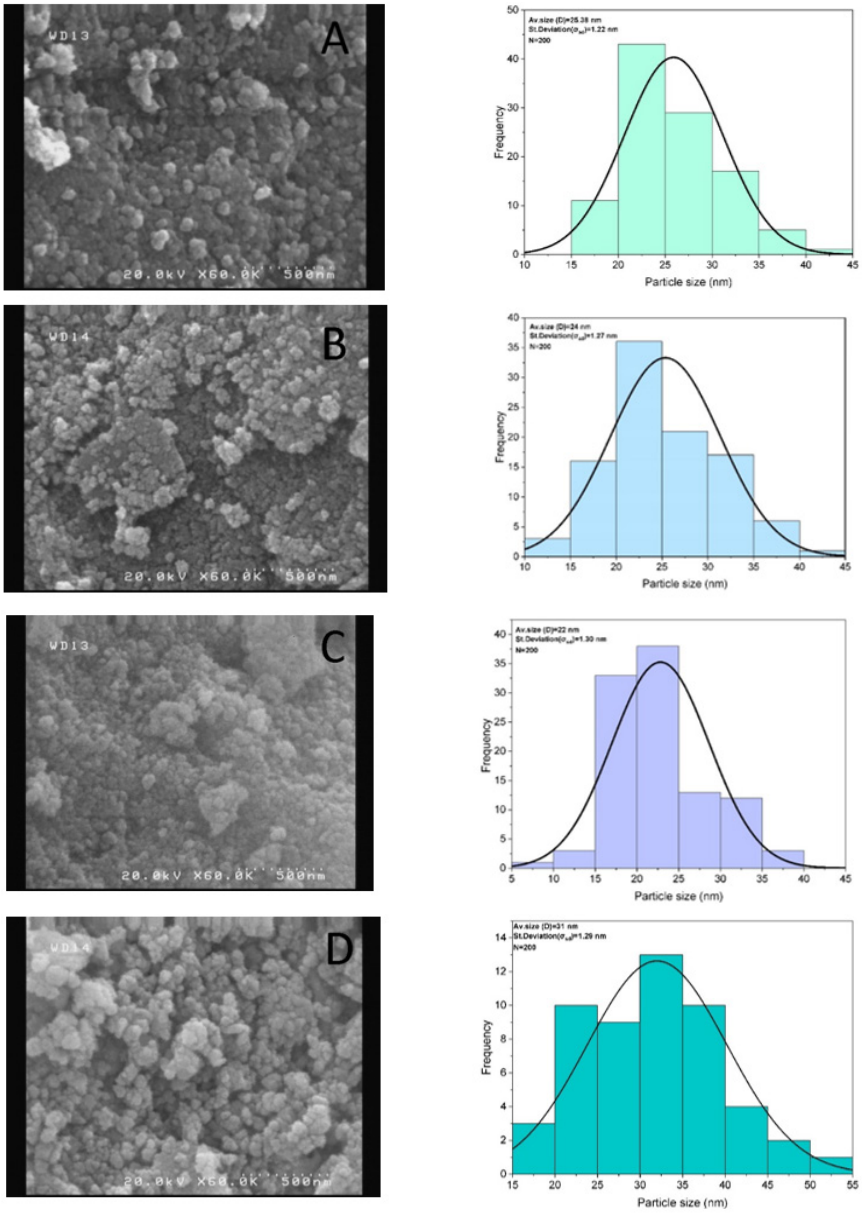

Fig. 9. FESEM images and particle size distribution histograms of A(CeO_2 NP (0.5:1)), B(CeO_2 NP (1:1)), C(CeO_2 NP (1.5:1)), and D(CeO_2 NP (2:1))

analysis revealed that as extract concentration increased from 10 to 30 mL, the average particle size decreased from 47 to 20 nm. Cerium oxide nanoparticles with similar morphological shape and uniform average particle size of less than 30 nm were synthesized using *Gloriosa superba* L. leaf extract [72], *Olea europaea* leaf extract [68], *Salvadora persica* extract [54] and *Moringa oleifera* leaf extract [58].

The calculated crystallite size obtained from the XRD analysis was smaller in comparison with the size observed through FESEM imaging. The observed discrepancy can be related to the fact that Scherrer's equation quantifies crystallite sizes as the sizes of "coherently diffracting domains" of crystals, but grains may encompass many of these domains [73]. Another possible reason for this difference can be ascribed to the aggregation of the nanoparticles caused by the magnetic interactions among them [74].

Fig. 10 shows the EDX spectrum of cerium oxide nanoparticles created by different concentrations

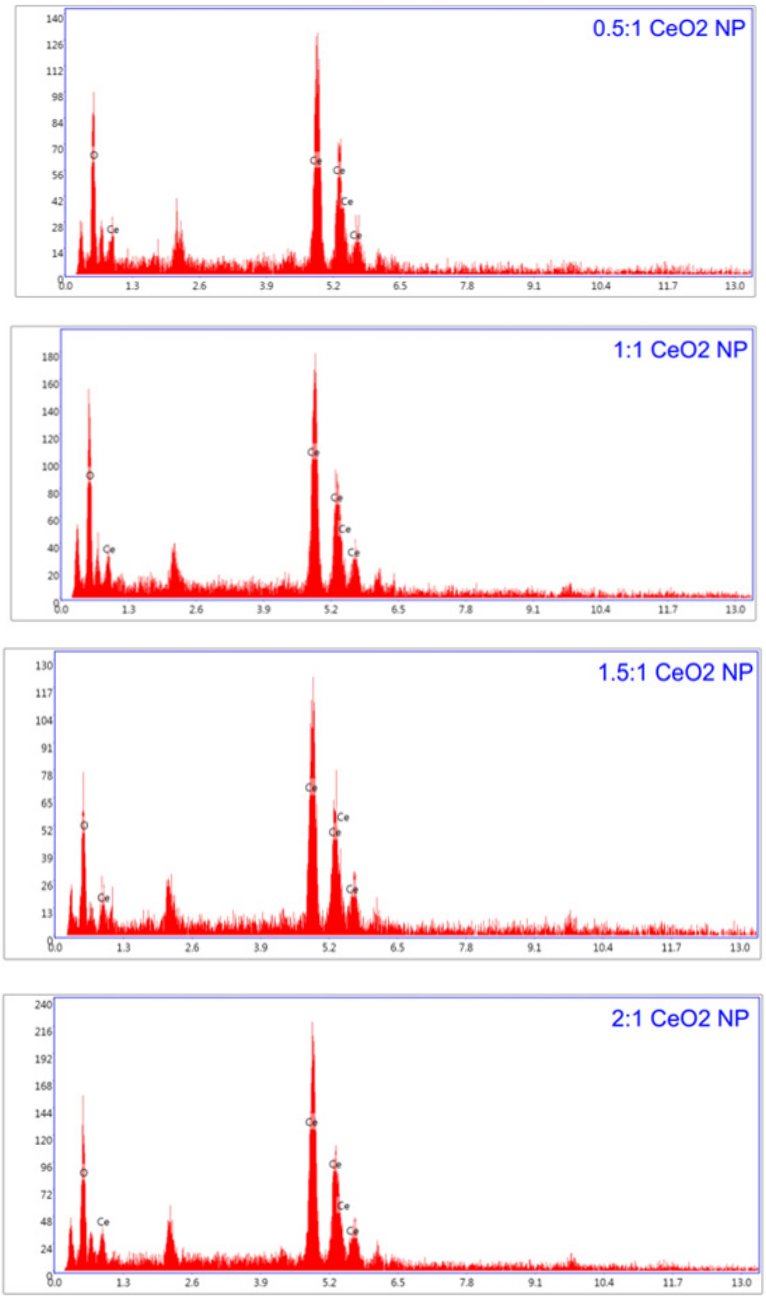

Fig. 10 EDX spectrums of CeO_2 nanoparticles

of *E. ramosissimum Desf* extract. The EDX graphs of all samples clearly show high-intensity peaks corresponding to Ce and O atoms in a specific energy of 20 keV. The absence of any other elements in the EDX spectrum confirms the successful biosynthesis of cerium oxide nanoparticles with no impurity in their compositions, the situation was confirmed by PXRD as well. Similar findings were reported for the biosynthesizing of cerium oxide nanoparticles [30, 46, 64, 75]. Since this experiment was carried out by preparing the sample through its deposition on double side adhesive carbon tape and coated with gold, the carbon and gold characteristic peaks were always present in the EDX spectra.

Dynamic Light Scattering (DLS) and zeta potential analysis

The analysis of the particle size distribution in the samples was conducted using the Dynamic Light Scattering (DLS) approach, which measures the hydrodynamic radius of each particle assuming they behave as individual spheres undergoing Brownian motion[76]. Furthermore, the Dynamic Light Scattering (DLS) technique is primarily employed for the measurement of particle size and the determination of shell thickness of a capping or stabilizing chemical involved in the formation of metallic nanoparticles[77].

The size distribution for all samples is shown in Fig. 11 in the form of a line graph. As illustrated from the graphs, particles showed a narrow size distribution which is within the range of 1-100 nm. The DLS analysis demonstrated average hydrodynamic diameter for cerium oxide nanoparticles were estimated to be 28.11 nm, 31.5nm, 25.34 nm, and 54.65 nm along with a Polydispersity index of 12.60%, 18.40%, 5%, and 25.10% respectively. The polydispersity index of 5% in group 3 indicates that the particles are nearly monodispersed. As the PDI index increases, the percentage of monodispersed particles will be decreased [78]. Based on the findings, the diameter of nanoparticles was not considerably different by raising the plant extract to 15 mL. However, when the concentration is increased to 20 mL, the particle size approximately doubles.

The obtained particle size by this technique was very close to FESEM analysis results. Meanwhile, these size values were over-expressed than those measured from XRD patterns. The possible explanation for this discrepancy may be attributed to that, crystallite size represents the average size of individual grains, whereas the particle size obtained via DLS analysis refers to the size of particles that are made up of several grains[79]. In addition to that, the size acquired through Dynamic Light Scattering (DLS) is influenced not only by the metallic core of particles but also by the presence of capping proteins and enzymes surrounding the particles [80]. Comparable DLS values for green cerium oxide nanoparticles were reported in the literature [29, 46, 81].

Zeta potential is an assessment that measures the electric charge present on the surface of nanoparticles and has a direct impact on the stability of nanoparticles. Nanoparticles with Zeta

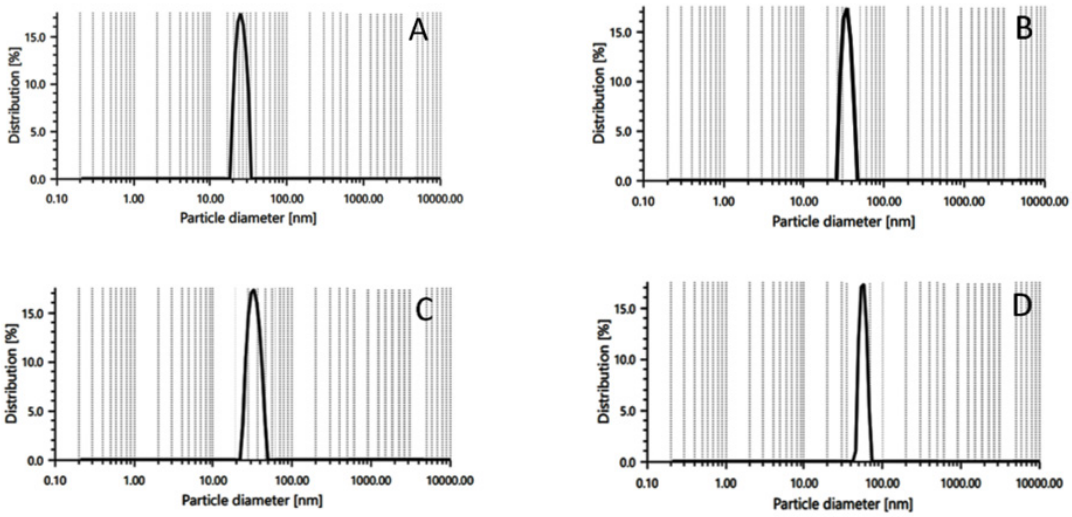

Fig. 11. Dynamic light scattering (DLS) patterns of *E. ramossisum Desf* mediated CeO_2NP A:(CeO_2 NP (0.5:1)), B:(CeO_2 NP (1:1)), C:(CeO_2 NP (1.5:1)) and D:(CeO_2 NP (2:1))

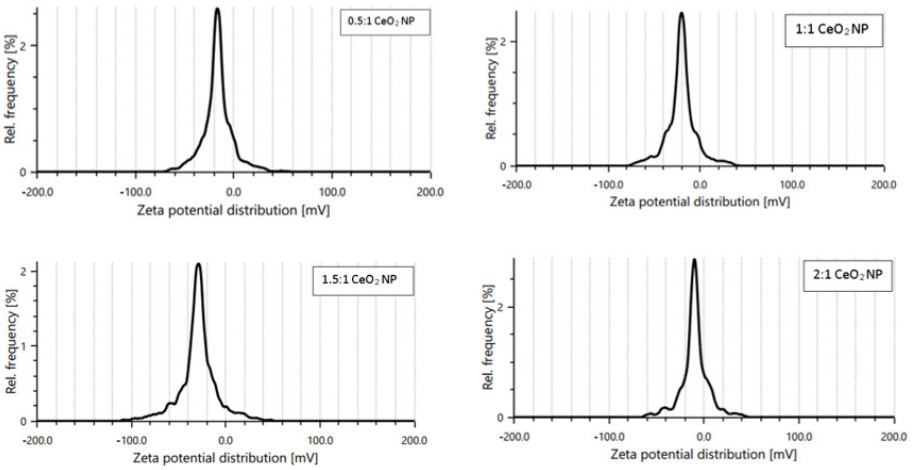

Fig. 12. Distribution of zeta potential of CeO2 NPs

potential values exceeding +25 mV or falling below -25 mV are generally regarded as having significant physical stability [82]. Fundamentally, the greater the absolute magnitude of zeta potential (whether positive or negative), the stronger the repulsion between the particles that to be aggregate, resulting in increased stability of the nanoparticles [83]. Fig. 12 displays the distribution of zeta potentials of E. r*amosissimum Desf* stabilized cerium oxide nanoparticles.

The mean zeta potential of CeO_2NPs prepared by different concentrations of E. ramosissimum Desf (5-20 mL) was measured to be -18 mV, -20.1 mV, -29.2 mV, and -11.4 mV respectively. The -29.2 mV, zeta potential value of (1.5:1 v/v) cerium oxide nanoparticle indicates its colloidal stability in suspension. The surface capping of CeO_2-NPs primarily consists of negatively charged groups, contributing significantly to the moderate stability of the nanoparticles as confirmed by the high negative values of zeta potential [29]. Conversely, zeta potential values of remaining three groups less than -25 mV, confirm particles had agglomeration. This finding could explain the increasing particle size as a result of agglomeration, as demonstrated by FESEM and DLS analysis in previous sections.

Nanoceria with similar zeta potential values were produced by utilizing aqueous leaf extracts of *S. nigrum* (-25.83 mV), *Mentha royleana* (<-28 mV), and *Pelargonium hortorum* (-25.8 mV) [29, 46, 84].

According to the above discussion, the sample that was prepared with 15 mL *E. ramosissimum Desf* extract had the sharpest charge transfer peak, bigger band gap energy, highly pure small crystallite size, uniform spherical morphology, and smallest particle size with high zeta potential value had been chosen as a suitable model for subsequent investigations.

Antibacterial study

Antibacterial activity of cerium oxide nanoparticles

Recent studies have indicated the potential utilization of cerium oxide nanoparticles as antimicrobial agents owing to their reduced toxicity, heat resistance, and capacity to absorb UV/Vis radiation[85]. Nanoparticles produced using green methods have demonstrated high effectiveness and relatively minimal harmful effects on healthy cells, in comparison to NPs created using different chemical processes[86].

The zone of inhibition was seen for different concentrations, as depicted in Fig. 13. The presence of inhibitory zones around samples demonstrated the antibacterial efficacy of CeO_2 nanoparticles

Fig.13. Inhibition zone of CeO_2 NPs against *Streptococcus mutans*

Table 2. Mean, standard deviation, and P value of zone of inhibition of different concentrations of CeO_2 NPs compared to control

	N	Mean (mm)	Std. Deviation	P-value
Control	5	15	0.7071	
2000 µg	5	32.6	1.517	<0.0001
1000 µg	5	25.2	1.643	<0.0001
500 µg	5	20.2	1.304	<0.0001
250 µg	5	0	0	<0.0001
125 µg	5	0	0	<0.0001
62.5 µg	5	0	0	<0.0001

at different concentrations. The biosynthesized CeO_2-NPs exhibit superior antibacterial activity compared to the chlorhexidine control group.

A promising zone of inhibition of 32.6, 25.2, and 20.2 mm was recorded at 2000 µg, 1000 µg, and 500 µg/mL concentrations respectively. Compared to the control group (15±0.7 mm), three concentrations of cerium oxide nanoparticles showed greater ZOI. It also showed that the last three concentrations had no antibacterial effect against streptococcus mutans. The mean, standard deviation, and P-value of the inhibition zone are presented in Table 2.

The findings indicate that the green CeO_2NPs possess a potent antibacterial effect, as an inhibition zone value of 10-20 mm is considered strong, while an inhibition zone above 20 mm is rated as extremely strong[87]. Furthermore, these results clearly showed that there is a direct correlation between the concentration of CeO_2 nanostructure samples and the size of the zone of inhibition found in bacterial growth, as concentration increased the zone of inhibition also increased. This implies that the antibacterial activity of CeO_2-mediated *E. ramosissimum Desf* is vastly dependent on the concentration of nanoparticles.

Table 3 presents the antibacterial activity of green CeO_2NPs prepared using different types of plant extracts. It is shown that the CeO_2NPs synthesized in this study using *E. ramosissimum Desf* exhibited a larger inhibition zone compared to the samples used in the prior investigations. Furthermore, variations in the dose of CeO_2NPs and testing methods result in distinct antibacterial characteristics.

The antibacterial activities of CeO_2NPs in the current study surpassed those documented in prior investigations. This could be attributed to the small particle size and crystallite size, as indicated by the analysis results from SEM, DLS, and XRD.

Different mechanisms are proposed for the antibacterial activity of cerium oxide nanoparticles. The potential of CeO_2 NPs against microorganisms is mostly influenced by its higher surface-to-volume ratio. A reduction in particle size increases the specific surface area, hence offering a greater number of active sites for interaction with bacterial cells. In addition, the smaller particles have a greater ability to enter the bacterial cells, leading to their disruption. [58]. Furthermore, the antibacterial activity of CeO_2NPs is primarily attributed to the electrostatic interaction between the positively charged nanoparticles and the negatively charged bacterial cell surface. The nanoparticles possess photocatalytic capabilities, which account for their antibacterial action. This interaction not only hampers the growth of bacteria but also triggers the production of reactive oxygen species (ROS), resulting in the death of cells [89-91]. The basic mechanism of photogeneration of ROS by CeO_2 NPs discussed as follows:

ROS were produced through a reaction known as the reduction and oxidation process. Cerium oxide nanoparticles function as semiconductors, absorbing photons when exposed to light with photon energy equal to or greater than the band gap energy. When illuminated by light, the electrons (e−) shift from the valence band to the conduction band resulting in the creation of holes (h+) within the valence band. The electrons and holes created by the photo induce reduction and oxidation reactions. When the electron interacts with oxygen, it generates the superoxide anion ($O2^{\bullet-}$), which is referred to as the reduction process. In addition, the holes undergo a reaction with hydroxyl ions, resulting in the production of hydroxyl radicals (•OH) through the process of oxidation. Furthermore, the presence of superoxide anions in water generates singlet oxygen ($^1O_2$) as a byproduct. These byproducts are known as reactive oxygen species [92]. Once the ROS interact with the bacterial cell wall and enter the cell, they will interact with the internal organelle of a cell including mesosome, cytoplasm, protein, and nucleoid, leading to malfunctioning and death of the cell [93].

Other possible mechanisms proposed for the antibacterial effect of nanoparticles include mechanical damage to the cell wall of

Table 3. Antibacterial activity of CeO2 NPs prepared using different plant extracts compared to present work

Precursors	Particle size(nm)	NPs concentration	Bacteria	ZOI (mm)	Ref.
Cerium chloride hepta hydrate and *Acalypha indica* leaf extract	36.2 *	100 mg/mL	*E. Coli*	9	[88]
			S. Aureus	17	
Cerium nitrate hexahydrate and *Olea europaea* leaf extract	24**	20 µg/5 µL ^	*E. Coli*	19	[68]
	6*		*S. Aureus*	10	
			K. pneumonia	9	
			P. aeruginosa	8	
Cerium nitrate hexahydrate and *Abelmoschus esculentus* Extract	30*	30 µg/mL ^^	*S. Aureus*	21	[34]
	36**		*K. pneumonia*	19	
Cerium nitrate hexahydrate and *Leucas aspera* leaf extract	4.6*	1000 µg/well^^	*K.aerogenes*	2.33	[27]
			P. desmolyticum	1.67	
			E. Coli	4.67	
			S. Aureus	3.33	
Cerium chloride hepta hydrate and *P. juliflora* leaf extract	11.42*	100 mg/mL^	*S. Aureus*	12.43	[56]
	3.7***		*S. pneumonia*	14.56	
			P. aeruginosa	4.09	
			P. vulgaris	4.38	
Cerium chloride hepta hydrate and *Azadirachta indica* leaf extract	7.61*	50 mg/ml^^	*B.subtilis*	11	[52]
			B.cereus	3	
			P. aeruginosa	14	
			K. pneumonia	0	
Cerium chloride hepta hydrate and *Gloriosa superba L.* leaf extract	24*	100 mg/mL^	*S. Aureus*	5.33	[72]
			S. pneumonia	4.67	
			E. Coli	4	
			P. aeruginosa	4.67	
			P. vulgaris	4.67	
			K. pneumonia	4.67	
			S.dysenteriae	4.33	
Cerium nitrate hexahydrate and *watermelon juice*	36*	1000 µg/µL^^	*K.aerogenes*	1	[69]
			S.aureous	1.47	
Ceric Ammonium Nitrate and *Moringa oleifera peel* extract	40-45*	25 µL^^	*E. Coli*	7	[59]
			S. Aureus	5	
Cerium chloride hepta hydrate and *Solanum nigrum leaf* extract	10.08*	100 µl ^	*B.subtilis*	21	[29]
	20**		*S. Aureus*	20	
	45***		*E. Coli*	22	
			P. aeruginosa	19	
Cerium chloride hepta hydrate and *Calotropis procera flower* extract	7.08*	100 µg/mL ^^	*B.subtilis*	13	[71]
	21**		*S. saprophyticus*	14	
			E. Coli	17	
			P. aeruginosa	15	
Cerium nitrate hexahydrate and *Moringa oleifera leaf* extract	11*	100 mg/mL	*S. Aureus*	22	[58]
	17**		*P. aeruginosa*	16	
			E. Coli	15	
Cerium nitrate hexahydrate and *Equisetum ramosissimum Desf*	5.99*	2000 µg/mL^^	*Streptococcus mutans*	32.6	Present study
	22**				
	25.34***				

bacteria through the rough surface of NPs [94]. Furthermore, it is believed that nanoparticles release an ion. Ions released by nanomaterial may interact with the thiol groups (-SH) of the proteins on the bactericidal cell surface, leading to the destruction of protein and loss of cell membrane permeability which in turn leads to cell death[95].

The experimental findings demonstrate that cerium oxide nanoparticles exhibit potent inhibitory effects on streptococcus mutans growth, rendering them suitable for many applications in the field of dentistry.

CONCLUSION

The findings from this study highlight the efficacy of *E. ramosissimum Desf* extract as a

proficient chelating agent for the eco-friendly synthesis of uniformly sized CeO_2 nanoparticles with strong antibacterial activity against cariogenic *S. mutans*. The demonstrated antibacterial efficacy supports the recommendation of green nanoceria as a potential antimicrobial agent in addressing dental caries, potentially extending its application to mouthwash, toothpaste, and dental resin composite formulations. It is imperative to conduct toxicity assessments before integrating these nanoparticles into consumer products. Additionally, comprehensive clinical trials are essential to evaluate the effectiveness of such products in preventing dental caries.

ACKNOWLEDGMENTS

The authors would like to thank the postgraduate research center of the College of Pharmacy at Hawler Medical University and the University of Tehran, College of Engineering, School of Electrical and Computer Engineering for providing the essential laboratory facilities, technical assistance, and resources crucial for conducting this research.

FUNDING

The study was conducted without financial assistance or funding from any agency or organization.

CONFLICT OF INTEREST

The authors declare that they have no conflict of interest.

REFERENCES

1. Petersen PE, Bourgeois D, Ogawa H, Estupinan-Day S, Ndiaye C. The global burden of oral diseases and risks to oral health. Bull World Health Organ. 2005; 83(9):661-669
2. Plonka KA, Pukallus ML, Barnett AG, Walsh LJ, Holcombe TH, Seow WK. Mutans streptococci and lactobacilli colonization in predentate children from the neonatal period to seven months of age. Caries Res. 2012;46(3):213-220.
3. Arthur RA, Cury AA, Graner RO, Rosalen PL, Vale GC, Paes Leme AF, et al. Genotypic and phenotypic analysis of S. mutans isolated from dental biofilms formed in vivo under high cariogenic conditions. Braz Dent J. 2011;22(4):267-274.
4. Aidara AW, Bourgeois D.Prevalence of dental caries: national pilot study comparing the severity of decay (CAO) vs ICDAS index in Senegal. Odontostomatol Trop. 2014;37(145):53-63.
5. Al-Darwish M, El Ansari W, Bener A. Prevalence of dental caries among 12-14 year old children in Qatar. Saudi Dent J. 2014;26(3):115-125.
6. Ajami BM, Hosseinzade H, Fazlibazaz BS, Velayatipour H. Evaluation of the antimicrobial activity of aqueous and alcoholic extracts of saffron stigma on oral pathogenic microbes (Streptococcus mutans, Lactobacillus, Candida albicans). Avicenna J Phytomed. 2015;5:7.
7. Naqvi SZ, Kiran U, Ali MI, Jamal A, Hameed A, Ahmed S, Ali N. Combined efficacy of biologically synthesized silver nanoparticles and different antibiotics against multidrug-resistant bacteria. Int J Nanomedicine. 2013; 8:3187-3195.
8. Abou Neel EA, Bozec L, Perez RA, Kim HW, Knowles JC. Nanotechnology in dentistry: prevention, diagnosis, and therapy. Int J Nanomedicine. 2015;10:6371-6394.
9. Wang L, Hu C, Shao L. The antimicrobial activity of nanoparticles: present situation and prospects for the future. Int J Nanomedicine. 2017;12:1227-1249.
10. Subhan MA. Antibacterial property of metal oxide-based nanomaterials. Nanotoxicity. 2020 :283-300.
11. I ST, Pitchiah S, Suresh V, Ramasamy P. Synthesis of zinc oxide nanoparticles from aqueous extract of Avicennia marina mangrove leaves and their antibacterial activities against oral pathogens. Cureus. 2023;15(10):47627.
12. Ramya G, Rajasekar A. Enhanced antibacterial effect of titanium dioxide nanoparticles mediated grape seed extract on oral pathogens-Streptococcus mutans and lactobacillus. J Evol Med Dent Sci. 2021;10(22):1656-1662
13. Gurunathan S. Rapid biological synthesis of silver nanoparticles and their enhanced antibacterial effects against Escherichia fergusonii and Streptococcus mutans. Arab J Chem. 2019;12(2):168-180.
14. Rajagopal S, Sugumaran S. The Antibacterial Effectiveness of Citrullus lanatus-Mediated Stannous Nanoparticles on Streptococcus mutans. Cureus. 2023;15(9):45504
15. Cheisson T, Kersey KD, Mahieu N, McSkimming A, Gau MR, Carroll PJ ,et al. Multiple Bonding in Lanthanides and Actinides: Direct Comparison of Covalency in Thorium(IV)- and Cerium(IV)-Imido Complexes. J Am Chem Soc. 2019;141(23):9185-9190.
16. Jairam LS, Chandrashekar A, Prabhu TN, Kotha SB, Girish M, Devraj IM, et al. A review on biomedical and dental applications of cerium oxide nanoparticles—Unearthing the potential of this rare earth metal. Journal of Rare Earths. 2023;41(11): 1645-1661.
17. Duan H, Wang D, Li Y. Green chemistry for nanoparticle synthesis. Chem Soc Rev. 2015; 44(16):5778-5792.
18. Singh J, Dutta T, Kim KH, Rawat M, Samddar P, Kumar P. 'Green' synthesis of metals and their oxide nanoparticles: applications for environmental remediation. J Nanobiotechnology. 2018; 16(1):84.
19. Shafey AME. Green synthesis of metal and metal oxide nanoparticles from plant leaf extracts and their applications: A review. Green Processing and Synthesis. 2020;9(1):304-339.
20. Altundag E, Ozturk M. Ethnomedicinal studies on the plant resources of east Anatolia, Turkey.Procedia Soc Behav Sci. 2011;19:756-777.
21. Jain AD. Jain S, Shrivastava. A short review on pharmacological activity of Equisetum ramosissimum. Asian J Pharm Clin Res. 2016; 5:1 8.
22. Boeing T, Tafarelo Moreno KG, Gasparotto Junior A, Mota da Silva L, de Souza P. Phytochemistry and Pharmacology of the Genus Equisetum (Equisetaceae): A Narrative Review of the Species with Therapeutic Potential for Kidney Diseases. Evid Based Complement Alternat Med. 2021; 2021:6658434.
23. Ismail AM, Ouaid T, Al-Amery M, Maulood B, Serson W. A preliminary study of phytochemicals in Equisetum arvense & E. ramosissimum (Equisetaceae) extracts from Northern Iraq. Fern Gaz. 2020; 21(3):115-121.
24. Savaya NSA, Issa RA, Talib WH. *In vitro* evaluation of the antioxidant, anti-Propioni bacterium acne and antityrosinase

effects of Equisetum ramosissimum (Jordanian horsetail). Trop J Pharm Res. 2020;19(10):2147-2152.
25. Sureshkumar J, Amalraj S, Murugan R, Tamilselvan A, Krupa J, Sriramavaratharajan V, et al. Chemical profiling and antioxidant activity of Equisetum ramosissimum Desf. stem extract, a potential traditional medicinal plant for urinary tract infections. Futur J Pharm Sci. 2021;7:1-11.
26. Harborne A. Phytochemical methods a guide to modern techniques of plant analysis: springer science & business media; 1998.
27. Malleshappa J, Nagabhushana H, Sharma SC, Vidya YS, Anantharaju KS, Prashantha SC, et al. Leucas aspera mediated multifunctional CeO_2 nanoparticles: Structural, photoluminescent, photocatalytic and antibacterial properties. Spectrochim Acta A Mol Biomol Spectrosc. 2015; 149:452-462.
28. Elahi B, Mirzaee M, Darroudi M, Oskuee RK, Sadri K, Amiri MS. Preparation of cerium oxide nanoparticles in Salvia Macrosiphon Boiss seeds extract and investigation of their photo-catalytic activities. Ceram Int. 2019; 45(4):4790-4797.
29. Muthuvel A, Jothibas M, Manoharan C, Jayakumar SJ. Synthesis of CeO 2-NPs by chemical and biological methods and their photocatalytic, antibacterial and in vitro antioxidant activity. Res Chem Intermed. 2020; 46:2705-2729.
30. Miri A, Beiki H, Najafidoust A, Khatami M, Sarani M. Cerium oxide nanoparticles: green synthesis using Banana peel, cytotoxic effect, UV protection and their photocatalytic activity. Bioprocess Biosyst Eng. 2021; 44(9):1891-1899.
31. Gu H, Soucek MD. Preparation and characterization of monodisperse cerium oxide nanoparticles in hydrocarbon solvents. Chem. Mater. 2007; 19(5):1103-1110.
32. Altaf M, Manoharadas S, Zeyad MT. Green synthesis of cerium oxide nanoparticles using Acorus calamus extract and their antibiofilm activity against bacterial pathogens. Microsc Res Tech. 2021; 84(8):1638-1648.
33. Paswan SK, Kumari S, Kar M, Singh A, Pathak H, Borah J, et al. Optimization of structure-property relationships in nickel ferrite nanoparticles annealed at different temperature. J Phys Chem Solids. 2021; 151:109928.
34. Ahmed HE, Iqbal Y, Aziz MH, Atif M, Batool Z, Hanif A, et al. Green Synthesis of CeO_2 Nanoparticles from the Abelmoschus esculentus Extract: Evaluation of Antioxidant, Anticancer, Antibacterial, and Wound-Healing Activities. Molecules. 2021; 26(15):4659.
35. Jain A, Shrivastava S. Extraction, isolation and characterization of bioactive components derived from whole plant of equisetum ramosissimum desf. J Adv Sci Res. 2020; 11(3):97-102.
36. Telange DR, Patil AT, Tatode A, Bhoyar B. Development and Validation of UV Spectrophotometric Method for the Estimation of Kaempferol in Kaempferol: Hydrogenated Soy PhosphatidylCholine (HSPC) Complex. Pharm Methods. 2014; 5(1):34-38.
37. Aleixandre-Tudo JL, Du Toit W. The role of UV-visible spectroscopy for phenolic compounds quantification in winemaking. Frontiers and new trends in the science of fermented food and beverages. 2018:200-204.
38. Aguayo-Morales H, Sierra-Rivera CA, Claudio-Rizo JA, Cobos-Puc LE. horsetail (equisetum hyemale) extract accelerates wound healing in diabetic rats by modulating IL-10 and MCP-1 release and collagen synthesis. Pharmaceuticals. 2023; 16(4):514.
39. Kar S, Patel C, Santra S. Direct room temperature synthesis of valence state engineered ultra-small ceria nanoparticles: investigation on the role of ethylenediamine as a capping agent. J. Phys. Chem. C. 2009; 113(12):4862-4867.
40. Singh S, Dosani T, Karakoti AS, Kumar A, Seal S, Self WT. A phosphate-dependent shift in redox state of cerium oxide nanoparticles and its effects on catalytic properties. Biomaterials. 2011; 32(28):6745-6753.
41. Emsley J. Nature's building blocks: an AZ guide to the elements: Oxford University Press, USA; 2011.
42. Miri A, Sarani M. Biosynthesis, characterization and cytotoxic activity of CeO_2 nanoparticles. Ceram Int. 2018; 44(11):12642-12647.
43. Korotkova AM, Borisovna PO, Aleksandrovna GI, Bagdasarovna KD, Vladimirovich BD, Vladimirovich KD, et al. Green synthesis of cerium oxide particles in water extracts Petroselinum crispum. ISRN Nanomater. 2019;4(3):176-1790.
44. Sabouri Z, Sabouri M, Amiri MS, Khatami M, Darroudi M. Plant-based synthesis of cerium oxide nanoparticles using Rheum turkestanicum extract and evaluation of their cytotoxicity and photocatalytic properties. Materials Technology. 2022;37(8):555-568.
45. Yulizar Y, Juliyanto S, Apriandanu DOB, Surya RM. Novel sol-gel synthesis of CeO_2 nanoparticles using Morinda citrifolia L. fruit extracts: Structural and optical analysis. J Mol Struct. 2021; 1231:129904.
46. Mahabadi AG, Mirzakhani A, Azizi A, Chavoshi S, Khaghani S. Extracts of Pelargonium hortorum: A natural and efficient fluid for fast and eco-friendly biosynthesis of CeO_2 nanoparticles for antioxidant and photocatalytic applications. Inorg Chem Commun. 2021; 127:108553.
47. Carmignan F, Matias R, Carollo CA, Dourado DM, Fermiano MH, Silva BAK, et al. Efficacy of application of Equisetum pyramidale Goldm. hydrogel for tissue restoration of induced skin lesions in Wistar rats. Braz J Biol. 2020; 80(1):12-22.
48. Altameme HJ, Hameed IH, Abu-Serag NA. Analysis of bioactive phytochemical compounds of two medicinal plants, Equisetum arvense and Alchemila valgaris seed using gas chromatographymass spectrometry and fouriertransform infrared spectroscopy. Malays Appl Biol. 2015;44(4):47-58.
49. LD TCT. ATR-FTIR spectra fingerprinting of medicinal herbs extracts prepared using microwave extraction. AJMAP. 2017; 3(1):1-9.
50. Deyab MA, Mohsen Q, Guo L. Theoretical, chemical, and electrochemical studies of Equisetum arvense extract as an impactful inhibitor of steel corrosion in 2 M HCl electrolyte. Sci Rep. 2022; 12(1):2255.
51. Masłowski M, Miedzianowska J, Czylkowska A, Strzelec K. Horsetail (Equisetum Arvense) as a functional filler for natural rubber biocomposites. Materials (Basel). 2020; 13(11):2526.
52. Sathiyapriya R, Vijayakumar P, Rajesh S. Bio-fabrication of Cerium oxide nanoparticles using Azadirachta indica and their Antibacterial Activity. Int J Adv Sci Eng. 2020; 6:1462-1468.
53. Aseyd Nezhad S, Es-haghi A, Tabrizi MH. Green synthesis of cerium oxide nanoparticle using *Origanum majorana* L. leaf extract, its characterization and biological activities. Appl Organomet Chem. 2020; 34(2):5314.
54. Miri A, Darroudi M, Sarani M. Biosynthesis of cerium oxide nanoparticles and its cytotoxicity survey against colon cancer cell line. Appl Organomet Chem. 2020; 34(1):5308.
55. Lagashetty A, Ganiger SK, Preeti R, Reddy S, Pari M. Microwave-assisted green synthesis, characterization and adsorption studies on metal oxide nanoparticles

synthesized using Ficus benghalensis plant leaf extracts. New J. Chem. 2020;44: 14095-14102.
56. Arunachalam T, Karpagasundaram M, Rajarathinam N. Ultrasound assisted green synthesis of cerium oxide nanoparticles using Prosopis juliflora leaf extract and their structural, optical and antibacterial properties. Materials Science-Poland. 2017;35(4):791-798.
57. Maqbool Q, Nazar M, Maqbool A, Pervez MT, Jabeen N, Hussain T, et al. CuO and CeO_2 nanostructures green synthesized using olive leaf extract inhibits the growth of highly virulent multidrug resistant bacteria. Front Pharmacol. 2018; 9:987.
58. Putri GE, Rilda Y, Syukri S, Labanni A, Arief S. Highly antimicrobial activity of cerium oxide nanoparticles synthesized using Moringa oleifera leaf extract by a rapid green precipitation method. J Mater Res Technol. 2021; 15:2355-2364.
59. Surendra TV, Roopan SM. Photocatalytic and antibacterial properties of phytosynthesized CeO_2 NPs using Moringa oleifera peel extract. J Photochem Photobiol B. 2016; 161:122-128.
60. Sisubalan N, Ramkumar VS, Pugazhendhi A, Karthikeyan C, Indira K, Gopinath K, et al. ROS-mediated cytotoxic activity of ZnO and CeO_2 nanoparticles synthesized using the Rubia cordifolia L. leaf extract on MG-63 human osteosarcoma cell lines. Environ Sci Pollut Res Int. 2018; 25(11):10482-10492.
61. Sheela K, Madhusudhanan J, Thirumagal J, Chawla N, Jagannathan S, Ahamed MN. Biosynthesis and biological applications of cerium oxide nanoparticles. Annals of RSCB. 2021; 25(6):203–213.
62. Ahmad A, Javed MS, Khan S, Almutairi TM, Mohammed AAA, Luque R. Green synthesized Ag decorated CeO_2 nanoparticles: Efficient photocatalysts and potential antibacterial agents. Chemosphere. 2023; 310:136841.
63. Munirathnam R, Vidya Y, Manjunatha H, Manjunatha S, Sridhar K, Seenappa L, et al. Multifunctional Properties of Ocimumsanctum Linn Leaves Mediated Synthesis of Nanoceria. Materials Open. 2023; 1: 2350006.
64. Sebastiammal S, Sonia S, Henry J, Fathima AL. Green synthesis of cerium oxide nanoparticles using aloevera leaf extract and its optical properties. Warasan Songkhla Nakharin. 2021; 43(2):582.
65. Yulizar Y, Kusrini E, Apriandanu DOB, Nurdini N. Datura metel L. Leaves extract mediated CeO_2 nanoparticles: Synthesis, characterizations, and degradation activity of DPPH radical. Surf Interfaces. 2020; 19:100437.
66. Purushotham B, Surendra BS, TR SS, Prashantha SC. Eco-friendly synthesis of CeO_2 NPs using Aloe barbadensis Mill extract: Its biological and photocatalytic activities for industrial dye treatment applications. J Photochem Photobiol. 2021; 7:100038.
67. Sharma JK, Srivastava P, Ameen S, Akhtar MS, Sengupta S, Singh G. Phytoconstituents assisted green synthesis of cerium oxide nanoparticles for thermal decomposition and dye remediation. Mater Res Bull. 2017; 91:98- 107.
68. Maqbool Q, Nazar M, Naz S, Hussain T, Jabeen N, Kausar R, et al. Antimicrobial potential of green synthesized CeO_2 nanoparticles from Olea europaea leaf extract. Int J Nanomedicine. 2016; 11:5015-5025.
69. Reddy Yadav L, Manjunath K, Archana B, Madhu C, Raja Naika H, Nagabhushana H, et al. Fruit juice extract mediated synthesis of CeO 2 nanoparticles for antibacterial and photocatalytic activities. *EPJ Plus*. 2016; 131:1-10.
70. Ibrahim AM, Mohamed F, Al-Quraishy S, Abdel-Baki A-AS, Abdel-Tawab H. Green synthesis of Cerium oxide/Moringa oleifera seed extract nano-composite and its molluscicidsal activities against biomophalaria alexanderina. J King Saud Univ Sci. 2021; 33(3):101368.
71. Muthuvel A, Jothibas M, Mohana V, Manoharan C. Green synthesis of cerium oxide nanoparticles using Calotropis procera flower extract and their photocatalytic degradation and antibacterial activity. Inorg Chem Commun. 2020; 119:108086.
72. Arumugam A, Karthikeyan C, Haja Hameed AS, Gopinath K, Gowri S, Karthika V. Synthesis of cerium oxide nanoparticles using Gloriosa superba L. leaf extract and their structural, optical and antibacterial properties. Mater Sci Eng C Mater Biol Appl. 2015; 49:408-415.
73. Dimitrijević R, Cvetković O, Miodragović Z, Simić M, Manojlović D, Jović V. SEM/EDX and XRD characterization of silver nanocrystalline thin film prepared from organometallic solution precursor. J. Min. Metall. Sect. B-Metall. 2013; 49(1):91-95.
74. Jalili H, Aslibeiki B, Ghotbi Varzaneh A, Chernenko VA. The effect of magneto-crystalline anisotropy on the properties of hard and soft magnetic ferrite nanoparticles. Beilstein J Nanotechnol. 2019; 10:1348-1359.
75. Nazaripour E, Mousazadeh F, Moghadam MD, Najafi K, Borhani F, Sarani M, et al. Biosynthesis of lead oxide and cerium oxide nanoparticles and their cytotoxic activities against colon cancer cell line. Inorg Chem Commun. 2021;131:108800.
76. Zhu H, Xu J, Yichuan Y, Wang Z, Gao Y, Liu W, et al. Catalytic oxidation of soot on mesoporous ceria-based mixed oxides with cetyltrimethyl ammonium bromide (CTAB)-assisted synthesis. J Colloid Interface Sci. 2017; 508:1-13.
77. Mohamed AA, Fouda A, Abdel-Rahman MA, Hassan SE-D, El-Gamal MS, Salem SS, et al. Fungal strain impacts the shape, bioactivity and multifunctional properties of green synthesized zinc oxide nanoparticles. Biocatal Agric Biotechnol. 2019; 19:101103.
78. Sankar V, SalinRaj P, Athira R, Soumya RS, Raghu KG. Cerium nanoparticles synthesized using aqueous extract of Centella asiatica: characterization, determination of free radical scavenging activity and evaluation of efficacy against cardiomyoblast hypertrophy. RSC Adv. 2015; 5(27):21074-21083.
79. Wang Z, Zhu H, Ai L, Liu X, Lv M, Wang L, et al. Catalytic combustion of soot particulates over rare-earth substituted Ln2Sn2O7 pyrochlores (Ln=La, Nd and Sm). J Colloid Interface Sci. 2016; 478:209-216.
80. Aziz N, Fatma T, Varma A, Prasad R. Biogenic synthesis of silver nanoparticles using Scenedesmus abundans and evaluation of their antibacterial activity. Journal of Nanoparticles. 2014; 2014:1-6.
81. Priya GS, Kanneganti A, Kumar KA, Rao KV, Bykkam S. Biosynthesis of cerium oxide nanoparticles using Aloe barbadensis miller gel. Int J Sci Res Publ. 2014;4(6):199-224.
82. Takma DK, Bozkurt S, Koç M, Korel F, Nadeem HŞ. Characterization and encapsulation efficiency of zein nanoparticles loaded with chestnut fruit shell, cedar and sweetgum bark extracts. Food Hydrocoll Health. 2023; 4:100151.
83. Dutta D, Mukherjee R, Patra M, Banik M, Dasgupta R, Mukherjee M, et al. Green synthesized cerium oxide nanoparticle: A prospective drug against oxidative harm. Colloids Surf B Biointerfaces. 2016; 147:45-53.
84. Khan M, Sohail, Raja NI, Asad MJ, Mashwani ZU. Antioxidant and hypoglycemic potential of phytogenic cerium oxide nanoparticles. Sci Rep. 2023; 13(1):4514.

85. Putri GE, Arief S, Jamarun N, Gusti FR, Zainul R. Microstructural analysis and optical properties of nanocrystalline cerium oxides synthesized by precipitation method. Rasayan J Chem. 2019;12(1):85-90.
86. De Lima R, Seabra AB, Durán N. Silver nanoparticles: a brief review of cytotoxicity and genotoxicity of chemically and biogenically synthesized nanoparticles. J Appl Toxicol. 2012; 32(11):867-879.
87. Putri GE, Arief S, Jamarun N, Gusti FR, Sary AN. Characterization of Enhanced Antibacterial Effects of Silver Loaded Cerium oxide Catalyst. Orient J Chem. 2018; 34(6): 2895-2901.
88. Kannan S, Sundrarajan M. A green approach for the synthesis of a cerium oxide nanoparticle: characterization and antibacterial activity. Int J Nanosci. 2014; 13(03):1450018.
89. Unnithan AR, Sasikala ARK, Sathishkumar Y, Lee YS, Park CH, Kim CS. Nanoceria doped electrospun antibacterial composite mats for potential biomedical applications. Ceram Int. 2014; 40(8):12003-12012.
90. Gour A, Jain NK. Advances in green synthesis of nanoparticles. Artif Cells Nanomed Biotechnol. 2019; 47(1):844-851.
91. Labanni A, Zulhadjri Z, Handayani D, Ohya Y, Arief S. The effect of monoethanolamine as stabilizing agent in Uncaria gambir Roxb. mediated synthesis of silver nanoparticles and its antibacterial activity. J Dispersf Sci. 2019; 41(10): 1480–1487.
92. Burello E, Worth AP. A theoretical framework for predicting the oxidative stress potential of oxide nanoparticles. Nanotoxicology. 2011; 5(2):228-235.
93. Bhagat M, Anand R, Datt R, Gupta V, Arya S. Green synthesis of silver nanoparticles using aqueous extract of Rosa brunonii Lindl and their morphological, biological and photocatalytic characterizations. J Inorg Organomet Polym Mater. 2019; 29:1039-1047.
94. Wang X, Yang F, Yang W, Yang X. A study on the antibacterial activity of one-dimensional ZnO nanowire arrays: effects of the orientation and plane surface. Chem Commun (Camb). 2007;(42):4419-4421.
95. Tong GX, Du FF, Liang Y, Hu Q, Wu RN, Guan JG, et al. Polymorphous ZnO complex architectures: selective synthesis, mechanism, surface area and Zn-polar plane-codetermining antibacterial activity. J Mater Chem B. 2013; 1(4):454-463.